

# Na<sub>2</sub>IrO<sub>3</sub> as a spin-orbit-assisted antiferromagnetic insulator with a 350 meV gap

R. Comin,<sup>1</sup> G. Levy,<sup>1,2</sup> B. Ludbrook,<sup>1</sup> Z.-H. Zhu,<sup>1</sup> C.N. Veenstra,<sup>1</sup> J.A. Rosen,<sup>1</sup> Yogesh Singh,<sup>3</sup>  
 P. Gegenwart,<sup>4</sup> D. Stricker,<sup>5</sup> J.N. Hancock,<sup>5</sup> D. van der Marel,<sup>5</sup> I.S. Elfimov,<sup>1,2</sup> and A. Damascelli<sup>1,2,\*</sup>  
<sup>1</sup>*Department of Physics & Astronomy, University of British Columbia, Vancouver, British Columbia V6T 1Z1, Canada*  
<sup>2</sup>*Quantum Matter Institute, University of British Columbia, Vancouver, British Columbia V6T 1Z4, Canada*  
<sup>3</sup>*Indian Institute of Science Education and Research (IISER) Mohali, Knowledge City, Sector 81, Mohali 140306, India*  
<sup>4</sup>*I. Physikalisches Institut, Georg-August-Universität Göttingen, D-37077 Göttingen, Germany*  
<sup>5</sup>*Département de Physique de la Matière Condensée, Université de Genève, CH-1211 Genève 4, Switzerland*  
 (Dated: March 11, 2019)

We study Na<sub>2</sub>IrO<sub>3</sub> by angle-resolved photoemission spectroscopy and in situ carrier doping via potassium deposition. From the K-induced chemical potential shift and the emergence of spectral weight across the insulating gap, together with complementary optical conductivity data, we estimate an optical gap  $\Delta_{eff} \simeq 350$  meV. By performing local-density approximation (LDA) band structure calculations, with the inclusion of spin-orbit coupling (SO) and Coulomb repulsion  $U$ , we determine that while the correct gap magnitude can only be reproduced by LDA+SO+ $U$ , the prodromes of an underlying insulating state are already found in LDA+SO. This challenges a simple Mott-Hubbard scenario, establishing Na<sub>2</sub>IrO<sub>3</sub> as a spin-orbit-assisted antiferromagnetic insulator.

PACS numbers: 71.20.Be, 74.25.Jb, 74.25.Gz, 71.15.Mb

The discovery of an effective  $J_{eff} = 1/2$  Mott-Hubbard state in Sr<sub>2</sub>IrO<sub>4</sub> [1] came as a surprise since this case departs from the established phenomenology of Mott-insulating behavior in the canonical early 3d transition-metal oxides, stemming from the very localized nature of the 3d electrons. In particular, it appears to violate the  $U > W$  Mott criterion, which for the very delocalized 5d Ir electrons is not fulfilled. It was proposed that the strong spin-orbit (SO) interaction in 5d systems ( $\zeta_{SO} \simeq 485$  meV for Ir [2]) might lead to instability against weak electron-electron correlation effects, and to the subsequent emergence of a many-body insulating ground state.

Since then iridates have become a burgeoning field of study, with Na<sub>2</sub>IrO<sub>3</sub> being one of the most recent members [3]. Starting from a  $J_{eff} = 1/2$  model in analogy with Sr<sub>2</sub>IrO<sub>4</sub>, this system was predicted to exhibit quantum spin Hall behaviour, and considered as a potential candidate to realize a topologically insulating state [4]. Further theoretical [5] and experimental [6] work highlighted the relevance of structural distortions lowering the local symmetry at the Ir site from octahedral ( $O_h$ ) to trigonal ( $D_{3h}$ ). Together with the structure comprised of edge-sharing IrO<sub>6</sub> octahedra, this leads to an effective bandwidth for the Ir 5d- $t_{2g}$  valence states of  $\sim 1$  eV. This potentially puts Na<sub>2</sub>IrO<sub>3</sub> closer to the  $U \sim W$  Mott criterion borderline - and thus to a Mott insulating phase - than the other iridates [5]. Transport, magnetic and calorimetric measurements revealed the bulk insulating nature, and found evidence for antiferromagnetic (AF) ordering at  $T_N \simeq 15$  K, together with a negative Curie-Weiss temperature ( $\theta \approx -120$  K) pointing to frustrated exchange interactions between the  $S = 1/2$  magnetic Ir<sup>4+</sup> ions [3]. Finally, resonant soft x-ray [7] and neutron scattering [6, 8] measurements, in conjunction with density functional theory (DFT) calculations [7], suggested that the underlying AF order follows an unconventional zig-

zag pattern, rather than simple Néel or stripy [9].

Na<sub>2</sub>IrO<sub>3</sub> has so far shown a complex and elusive behavior; in particular, the nature of its insulating ground state and the  $U/W$ /SO interplay are still highly debated. In this paper we present a study of the low-energy electronic structure by combining optics, angle-resolved photoemission spectroscopy (ARPES) with in-situ potassium doping, and DFT calculations in the local-density approximation (LDA). From the potassium-induced chemical potential shift and the emergence of spectral weight across the insulating gap in ARPES, we obtain the quantitative gap estimate  $\Delta_{eff} \simeq 350$  meV in excellent agreement with the optical conductivity. The LDA band structure calculations, performed for the most recently determined crystal structure [8] and with the inclusion of SO and  $U$ , indicate that while the precise gap magnitude can only be reproduced by LDA+SO+ $U$ , an insulating ground state is already present in LDA+SO: this establishes Na<sub>2</sub>IrO<sub>3</sub> as a spin-orbit-assisted antiferromagnetic insulator.

ARPES measurements were performed at UBC with 21.2 eV linearly polarized photons (He-I $\alpha$  line from a SPECS UVS300 monochromatized lamp) and a SPECS Phoibos 150 hemispherical analyzer. Energy and angular resolutions were set to 30 meV and 0.2°. Na<sub>2</sub>IrO<sub>3</sub> single crystals were grown by a self flux method [3] and pre-oriented by Laue diffraction; then cleaved in situ at a base pressure of  $5 \times 10^{-11}$  mbar, exposing the (001) surface (parallel to the Ir layers). During all measurements the temperature was kept at 130 K to avoid the onset of charging observed below 120 K. The complex optical conductivity was obtained at ambient conditions using combined reflectivity and ellipsometry measurements on the (001) surface of a freshly-cleaved crystalline platelet.

The 130 K angle-integrated valence-band photoemission spectrum of Na<sub>2</sub>IrO<sub>3</sub> in Fig. 1(a) shows two broad spectral features belonging to the Ir 5d- $t_{2g}$  bands (in the

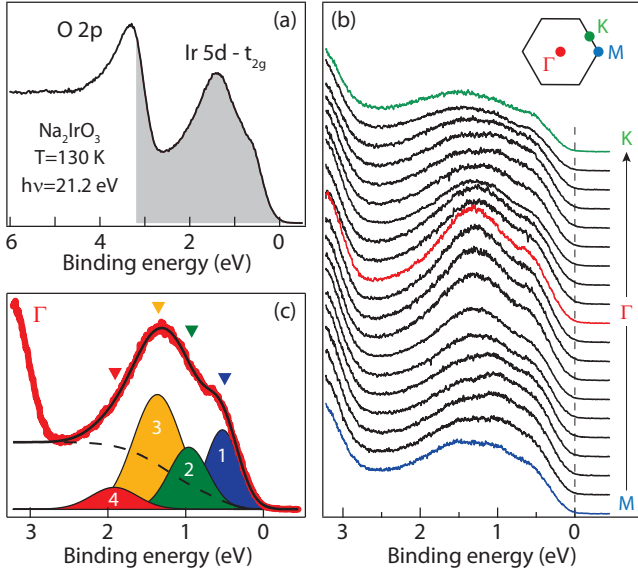


FIG. 1. (color online). (a) Angle-integrated O and Ir valence-band photoemission spectrum of Na<sub>2</sub>IrO<sub>3</sub>; the grey portion is shown in detail in (b,c). (b) ARPES energy distribution curves (EDCs) for the Ir 5d- $t_{2g}$  bands from along  $M-\Gamma-K$  (sketch of the Brillouin zone also shown). (c) Model fit of the  $\Gamma$ -point EDC with 4 Gaussian peaks for the Ir valence bands (VBs) and a Shirley background, with  $(E_{VB}, \Gamma_{VB}, \Delta E_{VB})$  in eV given by, from peak 1 to 4 over  $M-\Gamma-K$ : (0.50, 0.30, 0.06); (0.94, 0.39, 0.08); (1.39, 0.44, 0.09); (1.89, 0.43, 0.07).

0 to 3 eV binding energy range), and to the O 2p band (below 3 eV). Most importantly, the insulating character is evidenced by the lack of spectral weight at the chemical potential, which appears to be pinned to the top of the valence band. The ARPES data for the Ir 5d- $t_{2g}$  bands were acquired along the  $M-\Gamma-K$  high-symmetry directions in the first Brillouin zone, in both horizontal ( $p$ ) and vertical ( $s$ ) polarizations; however, no pronounced dependence was observed and the energy distribution curves (EDCs) in Fig. 1(b) are shown for  $p$  polarization only. One can see the absence of sharp energy-dispersing features, with the most obvious momentum-dependence being limited to the relative intensity of the main valence bands. EDCs were fitted using 4 Gaussian components [Fig. 1(c)], plus a Shirley-type background in order to account for secondary electrons (dashed black line). This choice is motivated by the fact that the 4-peak model is the one with best statistical likelihood (quantified via reduced  $\chi^2$ ) over the full set of experimental data, and also matches the number of density of states (DOS) features from DFT [Fig. 4(e,f)]. From the fit analysis over the whole momentum cut we find that the Ir 5d- $t_{2g}$  valence band (VB) dispersions do not exceed  $\Delta E_{VB} \sim 100$  meV in bandwidth, at variance with the expected larger hopping amplitude for  $t_{2g}$  states. On the other hand, a remarkable aspect of the Ir 5d- $t_{2g}$  features is their linewidth, with values  $\Gamma_{VB} = \sqrt{2}\sigma_{VB} \sim 300-450$  meV. A possible

origin might be structural disorder, consistent with the variable-range-hopping behavior of resistivity [3]. This might arise from the presence of stacking faults along the  $c$ -axis [8] and introduce an additional energy scale that will be important as the gap size is investigated (due to its comparable magnitude to SO,  $W$ , and  $U$ ). However, at this stage we cannot rule out other possible sources, such as e.g. strong electron-phonon coupling leading to polaronic behavior in the spectral function [10].

As for the size of the insulating gap, this cannot be readily identified by ARPES since photoemission can locate the valence band, as the first electron-removal state, but not the conduction band which belongs to the electron-addition part of the spectral function. To estimate the energy of the first electron-addition states, and in turn the size of the conductivity gap, our approach is to dope carriers (i.e., electrons) across the gap by in situ potassium deposition on the cleaved surfaces, and then follow by ARPES both the shift in chemical potential as well as the emergence of spectral weight corresponding to the induced conduction-band occupation. Typical results are summarized in Fig. 2 for K evaporation performed at 130 K on two different freshly cleaved surfaces, at a constant rate and in steps of equal exposure ( $I_{\text{evap}} = 4.2$  A/5 sec for sample 1;  $I_{\text{evap}} = 4.5$  A/30 sec for sample 2). Note that no K desorption between consecutive steps was observed, a sign of the stability of the evaporated surfaces at these temperatures.

The most obvious effect of K deposition is the shift towards higher binding energy of both Ir and O valence bands, as shown in Fig. 2(a) for the Ir 5d- $t_{2g}$  bands in particular. This effect arises from the equal and opposite shift of the chemical potential  $\Delta\mu$  when electrons donated by potassium are doped into the system. As shown in Fig. 2(c),  $\Delta\mu$  displays an initial rapid increase, then progressively reaches a saturation value of  $\sim 330$  meV. When the K-deposited spectra are shifted in energy by the corresponding  $\Delta\mu$  so that their high binding-energy trailing edges match the one of the fresh as-cleaved surface [Fig. 2(b)], one can observe the appearance of new spectral weight (SW) in the region close to and above the Fermi energy of the undoped compound. The low-energy K-induced spectral weight,  $\Delta SW$ , can be computed as:

$$\Delta SW = \int dk \int_{-1\text{eV}}^{E_F^+} dE [I(k, E, x_{K+}) - I(k, E, 0)] \quad (1)$$

where  $I(k, \omega)$  is the photoemission intensity,  $x_{K+}$  represents the K-induced surface doping, and  $E_F^+$  is the Fermi energy of the K-doped surface, which moves progressively beyond the undoped-surface  $E_F$ . The evolution of  $\Delta SW$  plotted as a function of  $\Delta\mu$  in the inset of Fig. 2(c) evidences a linear SW increase up to  $\Delta\mu \simeq 200-250$  meV, followed by a steeper rise once the saturation value  $\Delta\mu \simeq 330$  meV is being approached. This behavior can be understood as due to the initial

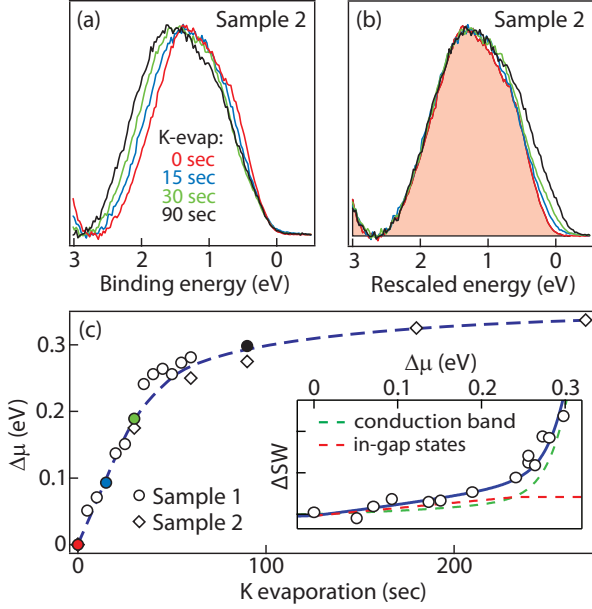


FIG. 2. (color online). (a) Background-subtracted angle-integrated EDCs for selected values of K-exposure [see colored markers in (c)]; the chemical potential shift  $\Delta\mu$  is revealed by the motion of the high binding-energy trailing edge. (b) Same as in (a), but shifted by the corresponding  $\Delta\mu$ . (c)  $\Delta\mu$  vs. K-deposition time for two different samples; inset: K-induced low-energy spectral weight  $\Delta SW$  as a function of  $\Delta\mu$ .

filling in of in-gap defect states – either pre-existing or induced by K deposition – which makes the jump of the chemical potential not as sudden as for a clean insulating DOS; correspondingly, the increase of spectral weight is marginal and for  $\Delta\mu < 250$  meV can be accounted for by a constant in-gap DOS [inset of Fig. 2(c), red dashed line]. Only when electronic states belonging to the Ir  $5d$ - $t_{2g}$  conduction band are reached one observes the saturation of  $\Delta\mu$  and a pronounced increase in  $\Delta SW$  [inset of Fig. 2(c), green dashed line]. This combined behavior points to an insulating gap of at least 330 meV.

Turning now to the optical conductivity data, in Fig. 3 we observe an insulating behavior with an absorption edge starting at 300–400 meV. We can fit the results using a joint DOS with Gaussian peaks for the conduction band (CB) and each of the 4 VBs (see caption of Fig. 1):

$$J(E) \propto \sum_{i=1}^4 \int dE' A_i G_{CB}(E' + E) G_{VB_i}(E'). \quad (2)$$

Here the prefactors  $A_i$  represent the optical transition strengths, with the band index  $i$  running over the 4 VB features extracted by ARPES, and are left free. A least-squares analysis returns  $E_{CB} \simeq 680$  meV. The consistency of the combined ARPES-optical conductivity analysis is confirmed by the onset of the simulated conduction band estimated following Ref. 10 as  $E_{CB}^{onset} = E_{CB} - 3\sigma_{CB} \simeq 340$  meV (with  $\sqrt{2}\sigma_{CB} = \Gamma_{CB} \simeq 160$  meV, a value consistent with LDA as shown later), thus very close to the

K-induced  $\Delta\mu$  saturation at 330 meV in ARPES. Note also how  $J(E)$  provides a good fit to the optical data in Fig. 3. Most important, the comprehensive analysis of photoemission and optical spectroscopy data indicates an effective conductivity gap magnitude  $\Delta_{eff} \simeq 350$  meV.

To understand the nature of  $\text{Na}_2\text{IrO}_3$  insulating state, we have performed band-structure calculations using the linearized augmented plane wave method in WIEN2K [11], and the most recently refined monoclinic  $C2/m$  crystal structure with 2 formula units per unit cell [8]. Exchange and correlation effects were treated within the generalized gradient approximation [12]; SO coupling was included as a second variational step using eigenfunctions from scalar relativistic calculation [13]. The LDA+U method was applied to the Ir  $5d$  states by varying  $U$  from 1 to 5 eV [14] with  $J_H = 0.6$  eV [15], and adopting the zigzag antiferromagnetic spin arrangement with moments along the  $a$  axis (zigzag- $a$ ) [7]. The  $k_z = 0$  band structure results from LDA, paramagnetic LDA+SO, and AF zigzag- $a$  LDA+SO+U ( $U = 3$  eV,  $J_H = 0.6$  eV) are shown in Fig. 4(a-c). For comparison, the LDA+SO+U results are superimposed to the ARPES intensity map from as-cleaved  $\text{Na}_2\text{IrO}_3$  (a doubling of bands is observed in LDA+SO+U due to the imposed AF ordering). Unlike the case of  $\text{Sr}_2\text{IrO}_4$ , the  $t_{2g}$  degeneracy is lifted due to structural distortions and the presence of Na in the Ir plane. The role of these structural features is revealed by the comparison with LDA calculations for a distortion- and Na-free hypothetical  $\text{IrO}_2$  parent compound: while in  $\text{IrO}_2$  the  $t_{2g}$ -dispersions are as wide as  $\sim 1.6$  eV (not shown), the Na-induced band folding in  $\text{Na}_2\text{IrO}_3$  opens large band gaps, leading to much narrower  $t_{2g}$ -subbands ( $\sim 100$  meV). Nonetheless, the material is still metallic in

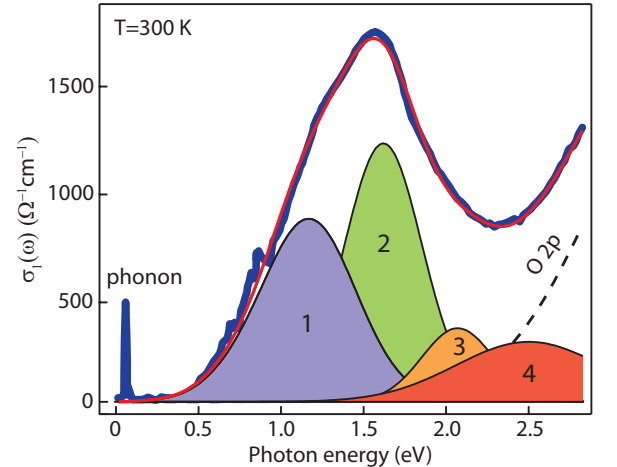


FIG. 3. (color online). Optical conductivity data (blue line), together with the simulated Ir  $5d$ - $t_{2g}$  joint particle-hole DOS (black line), and its individual components from the simultaneous fit of ARPES and optical data [colors and labels are consistent with the valence band features in Fig. 1(c), which are the initial states of the lowest-energy optical transitions].

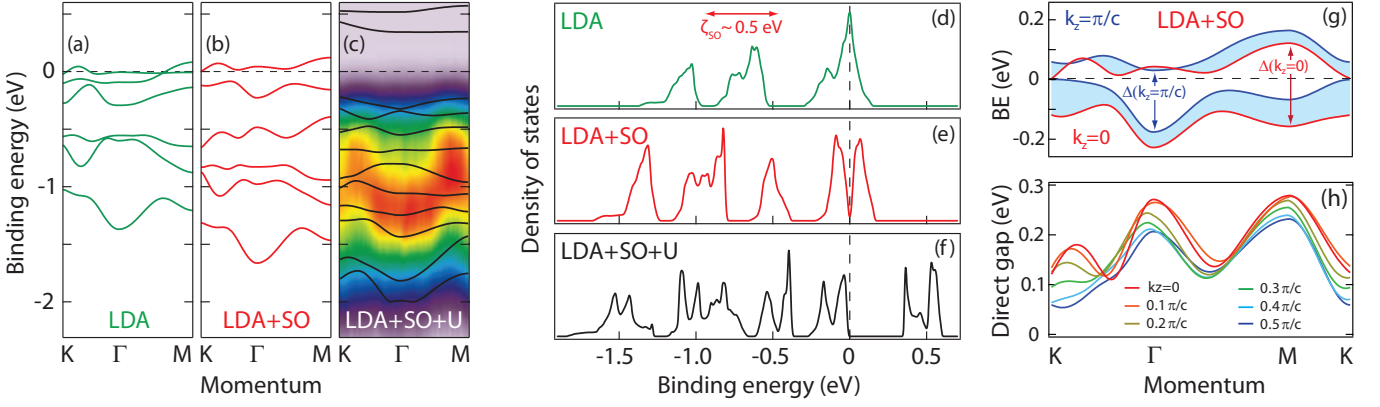


FIG. 4. (color online). (a-c) Ir 5d- $t_{2g}$  band structure ( $k_z = 0$ ), and (d-f) corresponding DOS, obtained with LDA, LDA+SO, and spin-averaged LDA+SO+U ( $U = 3$  eV,  $J_H = 0.6$  eV), respectively; in (c) the  $M - \Gamma - K$  ARPES data are also shown. (g)  $k_z$  dispersion, for the last occupied and first unoccupied Ir 5d- $t_{2g}$  bands from LDA+SO, as indicated by the filled region between the  $k_z = 0$  and  $\pi/c$  extreme lines; while the filled areas overlap, a direct gap (i.e.  $\Delta k = 0$ ) between valence and conduction bands is present for all  $k_z$  and  $k_{\parallel}$ . (h) LDA+SO direct gap distribution along  $M - \Gamma - K$ , for different  $k_z$  in the 3D Brillouin zone.

LDA with a high DOS at the Fermi level [Fig. 4(a,d)], at variance with the experimental observations.

Given such small  $t_{2g}$  bandwidths, one might expect the system to be even more unstable against local correlations than anticipated. Indeed, a good overall agreement with the data is found in LDA+SO+U for  $U = 3$  eV and  $J_H = 0.6$  eV [Fig. 4(c,f)]. While this seems to point to a classical Mott-Hubbard insulating state driven by electronic correlations, let us now examine more specifically the role played by SO. When SO is switched on in LDA – without the inclusion of U – the system turns immediately insulating as evidenced by the  $k_z = 0$  band dispersion in Fig. 4(b), although with a zero-conductivity-gap in the DOS [Fig. 4(e)]. A closer inspection of the LDA+SO dispersion for first occupied and unoccupied bands – versus both  $k_{\parallel}$  and  $k_z$  in Fig. 4(g) – reveals that the lack of a larger DOS gap stems from the overlap of VB( $k_z = \pi/c$ ) and CB( $k_z = 0$ ): i.e. the *indirect* (conductivity,  $\Delta k \neq 0$ ) gap is zero. On the other hand, as shown in Fig. 4(h), the *direct* (optical,  $\Delta k = 0$ ) gap is non-zero and – when both  $k_{\parallel}$  and  $k_z$  dispersions are taken into account – it ranges from a minimum of 54 meV to a maximum of 220 meV over the full Brillouin zone. Switching on U in LDA+SO simply moves occupied and unoccupied states apart in energy, opening a conductivity gap which scales linearly with  $U_{eff} = U - J_H$ . Instead, in LDA+U without SO (not shown), a large  $U_{eff} \simeq 1.5$  eV is needed before the conductivity gap starts opening. The depletion of electronic states at  $E_F$  in LDA+SO without the inclusion of U, and the linear scaling of the conductivity gap with  $U_{eff}$  in LDA+SO+U as opposed to the onset at  $U_{eff} \simeq 1.5$  eV in LDA+U, indicate that SO – rather than U – is the key interaction in driving the insulating state. Yet the closer quantitative agreement achieved with the inclusion of U suggests that underlying electronic correlations cannot be completely disregarded, consistent with

the local moment behavior observed well above  $T_N$  [3].

In conclusion, by combining ARPES observations of chemical potential shift with in situ carrier doping and optical conductivity results, we estimate the optical gap  $\Delta_{eff} \simeq 350$  meV. A detailed DFT analysis establishes  $\text{Na}_2\text{IrO}_3$  as a spin-orbit-assisted AF insulator, whose properties are governed by the delicate interplay between structural distortions, SO, and electronic correlations.

We acknowledge S. Bhattacharjee and G.A. Sawatzky for discussions, D. Wong and P. Dosanjh for technical assistance. The UBC work was supported by Killam, Sloan, CRC, and NSERC's Steacie Fellowship Programs (A.D.), NSERC, CFI, and CIFAR Quantum Materials.

\* damascelli@physics.ubc.ca

- [1] B. J. Kim *et al.*, Phys. Rev. Lett. **101**, 076402 (2008).
- [2] M. Montalti, A. Credi, L. Prodi, and M. T. Gandolfi, *Handbook of photochemistry - third edition* (CRC Press Taylor and Francis Group, 6000 Broken Sound Parkway NW, Suite 300 Boca Raton, FL 33487-2742, 2006).
- [3] Y. Singh and P. Gegenwart, Phys. Rev. B **82**, 064412 (2010).
- [4] A. Shitade *et al.*, Phys. Rev. Lett. **102**, 256403 (2009).
- [5] H. Jin *et al.*, arXiv:0907.0743v1 (2009).
- [6] F. Ye *et al.*, arXiv:1202.3995 (2012).
- [7] X. Liu *et al.*, Phys. Rev. B **83**, 220403 (2011).
- [8] S. K. Choi *et al.*, Phys. Rev. Lett. **108**, 127204 (2012).
- [9] J. Chaloupka *et al.*, Phys. Rev. Lett. **105**, 027204 (2010).
- [10] K. M. Shen *et al.*, Phys. Rev. Lett. **93**, 267002 (2004).
- [11] P. Blaha *et al.*, in *An augmented plane wave plus local orbitals program for calculating crystal properties*, edited by K. Schwarz (Technical University of Wien, 2001).
- [12] J. P. Perdew *et al.*, Phys. Rev. Lett. **77**, 3865 (1996).
- [13] A. H. MacDonald *et al.*, J. Phys. C Solid State Phys. **13**, 2675 (1980).
- [14] V. I. Anisimov *et al.*, Phys. Rev. B **48**, 16929 (1993).
- [15] D. van der Marel and G. A. Sawatzky, Phys. Rev. B **37**, 10674 (1988).